

# Analysis of the Fine Structure of the *D*-Exciton Shell in Cuprous Oxide

Julian Heckötter,\* Patric Rommel, Jörg Main, Marc Aßmann, and Manfred Bayer

The exciton states in cuprous oxide show a pronounced fine structure splitting associated with the crystal environment and the resulting electronic band structure. High-resolution spectroscopy reveals an especially pronounced splitting of the yellow *D* excitons with one state pushed above any other state with the same principal quantum number. This large splitting offset is related to a strong mixing of these *D* states with the *1S* exciton of the green series, as suggested by previously published calculations. Here, a detailed comparison of this theory with experimental data is given, which leads to a complete reassignment of the experimentally observed *D* exciton lines. The origin of different amounts of green admixture to *D*-envelope states is deduced by analyzing the different terms of the Hamiltonian. The yellow–green mixing leads to level repulsion and induces an exchange interaction splitting to *D*-envelope states, from which one of them becomes the highest state within each multiplet. Furthermore, the assignment of *D* exciton states according to their total angular momentum *F* is given and corrects an earlier description given in a former study.

the art of exciton spectroscopy: by resolving deviations of the exciton level spectrum in a  $\text{Cu}_2\text{O}$  bulk crystal from the hydrogen-like model, we show that detailed insight into the electronic band structure can be taken from such investigations.

Excitons have recently regained enhanced interest due to the emergence of materials with enhanced exciton binding energies so large, that they are even stable under ambient conditions. Examples of such material systems are transition metal dichalcogenides,<sup>[2]</sup> organic and inorganic perovskites,<sup>[3]</sup> and the various classes of colloidal nanocrystals.<sup>[4]</sup> However, also established model systems for excitons in optical spectra can provide essential contributions to the understanding of exciton physics as many features are universal, at least on a qualitative level, despite quantitative differences due to their varying binding

## 1. Introduction

Excitons determine the optical properties of semiconductors and insulators,<sup>[1]</sup> offering many interesting aspects for fundamental physics as well as technological applications. As such, they have been subject of countless manuscripts published during the 60 years of *physica status solidi*. It is hopeless to give a comprehensive overview of these studies. Instead, we give an example of the current state of

energies. Bulk cuprous oxide ( $\text{Cu}_2\text{O}$ ) as the material in which excitons were discovered has a prominent role in this respect because of the rich exciton spectrum to which multiple states contribute.


During recent years, high-resolution spectroscopy on  $\text{Cu}_2\text{O}$  has revealed detailed fine structure splittings of the yellow exciton states associated with a particular principal quantum number *n*. These findings have demonstrated that the standard hydrogen-like model description of a bulk exciton is not sufficient for an in-depth understanding of exciton levels, in case that the data-providing experiment gives sufficient insight. The reason is, coarsely spoken, the deviation of the crystal structure hosting the exciton from the isotropic vacuum due to its discrete symmetries.

Several factors contribute to the extraordinary position of cuprous oxide in exciton physics. First, natural, but also artificial crystals show a remarkable quality in terms of low defect concentration on the order of  $10^{10}\text{cm}^{-3}$ .<sup>[5]</sup> Second, the Rydberg energy of the exciton series is rather high with about  $\text{Ryd} = 90\text{ meV}$ . Third, the dipole-forbidden interband optical transitions result in a rather small oscillator strength, leading to narrow linewidths.<sup>[6]</sup> All these factors have enabled unprecedented insight into exciton fine structure splittings. Probably the first report on this fine structure was in the study by Fröhlich et al.,<sup>[7]</sup> in which two different experimental techniques, one-photon and two-photon absorption (OPA and TPA), gave access to different states in the exciton multiplet associated with a fixed *n*, but different orbital angular momenta *L* of the envelope wavefunction. Although mostly the states with *P*-type envelope show up in one-photon absorption, *S* and *D* excitons dominate the two-photon absorption spectra.

J. Heckötter, M. Aßmann, M. Bayer  
Experimentelle Physik 2  
Technische Universität Dortmund  
Dortmund 44221, Germany  
E-mail: julian.heckoetter@tu-dortmund.de

P. Rommel, J. Main  
Institut für Theoretische Physik 1  
Universität Stuttgart  
Stuttgart 70550, Germany

M. Bayer  
Ioffe Institute  
Russian Academy of Sciences  
St. Petersburg 194021, Russia

 The ORCID identification number(s) for the author(s) of this article can be found under <https://doi.org/10.1002/pssr.202100335>.

© 2021 The Authors. *physica status solidi* (RRL) Rapid Research Letters published by Wiley-VCH GmbH. This is an open access article under the terms of the Creative Commons Attribution License, which permits use, distribution and reproduction in any medium, provided the original work is properly cited.

DOI: 10.1002/pssr.202100335

In the study mentioned earlier, for each principal quantum number up to  $n = 5$ , a splitting between states with different  $L$  was observed, unexpected from the hydrogen model. The splitting energies decrease with increasing  $n$ . A detailed theoretical analysis by Uihlein et al.<sup>[8]</sup> related this splitting to the particular electronic band structure, namely of the valence band. The lowest conduction band has a parabolic dispersion to a very good approximation. For the holes, the dispersion is largely determined by the interaction of the two topmost valence bands which show a pronounced anticrossing for finite wavenumbers. As a consequence, both valence bands have strong deviations from parabolicity and isotropy. The two exciton series associated with the two valence bands, called the yellow and the green series, respectively, become intermixed.

Furthermore, the orbital angular momentum of the envelope, requiring rotational symmetry, is not fully appropriate to characterize exciton states. Indeed, a thorough analysis showed that the exciton Hamiltonian of cubic symmetry leads to a mixing of angular momentum eigenstates of either even or odd symmetry. That is, the excitons observed by TPA in the studies by Fröhlich et al. and Uihlein et al.<sup>[7,8]</sup> are not pure  $S$  or  $D$  states, but rather mixed  $S$ – $D$  states with different relative contents. For simplicity, we will, however, retain the simple one-letter notation according to the most prominent angular momentum quantum number in an exciton state.

In addition to the deviation from parabolicity in the valence band structure also the short-range electron–hole exchange interaction contributes to the exciton splitting.<sup>[7,8]</sup> As a contact interaction, the exchange affects the  $S$ -component of an exciton. Both factors result in the splitting pattern observed in experiment. Another origin for the observed splittings might be given by a polaritonic  $LT$  splitting.<sup>[9]</sup> However, as shown in the study by Stolz et al.,<sup>[6]</sup> these splittings are expected to occur for states at principal quantum numbers higher than  $n = 28$ . At lower  $n$ , they can be neglected due to the phonon-dominated broadening of lines and the weak light–matter coupling.

In the study by Fröhlich et al.,<sup>[7]</sup> however, no further splitting of each exciton shell defined by the quantum number tuple  $(n, L)$  could be resolved.

More than three decades after this first study, high-resolution OPA allowed not only for a significant extension of the exciton series to higher principal quantum numbers up to  $n = 25$  and  $30$ ,<sup>[10,11]</sup> but revealed also further details of their fine structure. Namely, for  $n > 3$ , on the high energy flank of the  $P$  excitons, the nominal  $F$  exciton multiplet could be observed for the same band structure reasons, as mentioned earlier.<sup>[12]</sup> The crystal Hamiltonian leads to a mixing of  $P$  and  $F$  states, shuffling oscillator strength to the latter. Therefore, also here, it would be more correct to refer to these excitons as mixed  $P$  –  $F$  states.

The  $F$  multiplet shows a threefold, almost equidistant splitting as small as  $10 \mu\text{eV}$  for  $n = 4$  and  $5$ . The linewidth of each feature is a few times smaller, because the oscillator strength remains more than two orders of magnitude below that of the  $P$  excitons. Still, there is large interest in high angular momentum states, because they potentially provide long exciton lifetimes, making them attractive for applications that require intermediate storage times.

With increasing  $n$ , the splitting strongly drops, so that signatures of  $F$  excitons could be found only up to  $n = 12$ . As the odd

exciton states are not affected by exchange, the splitting can be purely assigned to band mixing effects determined in leading order by quadratic combinations of hole momentum operator components along different directions. The corresponding interaction matrix elements scale as  $n^{-3}$ , in agreement with the experiment.<sup>[12]</sup>

The fine structure of other exciton shells  $(n, L)$  has not been discussed in detail so far, even though experiments clearly demonstrated such splittings, facilitated also by application of external electric or magnetic fields.<sup>[13–15]</sup> Most prominent is the case of the  $D$  excitons.

Since even parity  $D$  excitons are optically activated by electric fields, the details of their fine structure are of importance for the analysis of the high- $n$  regime close to the bandgap, where OPA spectra are influenced by the presence of inherent electric fields induced by charged impurities.<sup>[5,16]</sup> Moreover,  $D$  excitons show characteristic absorption features in OPA on synthetic samples with a certain amount of disorder.<sup>[17]</sup>

## 2. Fine Structure of $D$ Excitons

### 2.1. Assignment of Experimental Lines

The fine structure splitting of the  $D$  excitons could be accurately accessed in OPA studies by applying an additional external electric field to the sample in the study by Heckötter et al.<sup>[14]</sup> Here, we use that data and analyze the observed  $D$  exciton fine structure. For low fields, the  $D$  states become mixed dominantly with the lower energy  $P$  excitons of the same  $n$ , acquiring thereby oscillator strength so that they emerge in one-photon absorption spectra. At low field strengths their energies show almost no dependence on the electric field in this regime, because the Stark shift to lower energies and the high energy shift due to repulsion from the  $P$ -level mixing approximately compensate each other. This enables a rather precise determination of the state energies within the  $(n, D)$  multiplet at zero field. **Figure 1** shows contourplots of the second derivative of transmission spectra in electric fields for the  $n = 3$  and  $n = 4$  multiplets. We first discuss the multiplet of  $n = 3$ , see **Figure 1a**, the principal quantum number from which on the  $D$  excitons appear in the spectra, but higher angular momentum excitons, for example, like  $F$  excitons, do not yet contribute. For details on the experiment, we refer to the study by Heckötter et al.<sup>[14]</sup>

Without electric field, the transmission spectrum is dominated by the  $P$  exciton with some weak indication for the quadrupole-allowed  $S$  exciton on the low energy side. With increasing electric field three features show up on the high energy side of the  $P$  line that can be assigned to the  $D$  multiplet: a closely spaced doublet with a splitting of  $0.2 \text{ meV}$  and another feature on the high energy side split from the center of the doublet by more than  $1 \text{ meV}$ . This splitting is comparable with the splitting of the  $n = 3$   $S$  *ortho* and *para* states, which amounts to about  $1.2 \text{ meV}$ .

In total, the  $D$  multiplet consists of five states according to the possible angular momentum projections. Here, we observe three lines in OPA, at least in low electric fields, where field-induced state mixing remains rather weak. A first assignment of these lines was given by Schweiner et al.,<sup>[18]</sup> where detailed calculations

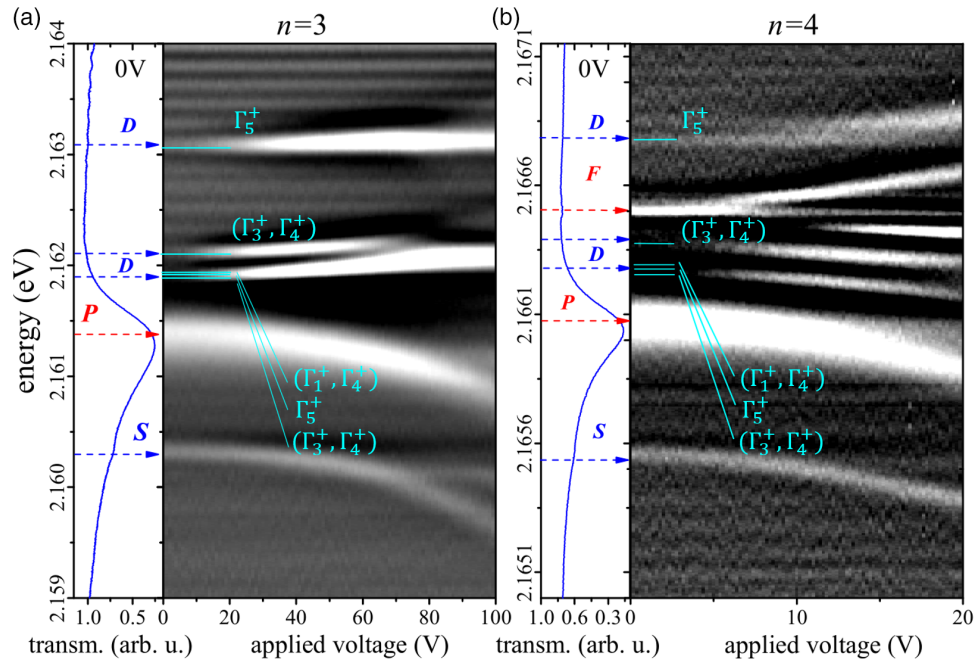


**Figure 1.** a,b) Comparison of contour plots of second derivatives of transmission spectra in the energy range around the  $n = 3$  (a) and  $n = 4$  (b) excitons versus applied bias. The left panels show for reference the zero-bias spectrum with the labels of the different envelope states. The blue lines indicate even excitons, the red lines odd excitons. In the right panels, calculated energies and corresponding symmetries for  $D$ -envelope states are indicated in cyan. a) For  $n = 3$ , the splitting of calculated  $D$  states agrees quite well with the three lines emerging with increasing electric field on the high energy flank of the  $P$  state in experiment: Of 5  $D$  states in total, three are found to be almost degenerate and match with the lowest one of the three lines observed in the spectra. The remaining two agree with the two separated lines at higher energies. The calculated values are shifted by  $-237 \mu\text{eV}$  for better overall agreement. b) For  $n = 4$ , the  $F$  excitons contribute to the multiplet. Still, the five calculated  $D$  states can be identified with three  $D$  lines observed in the spectra: two  $D$  lines emerge with increasing electric field in between the  $P$  and  $F$  states, from which the lowest one matches with the three lowest states of the calculation and the higher one matches with the calculated energy of the  $(\Gamma_3^+, \Gamma_4^+)$   $D$  exciton. The highest line observed in experiment agrees well with the calculated energy of the  $\Gamma_5^+$   $D$  exciton. Remarkably, it lays above the  $F$  states. The calculated energies are shifted by  $-218 \mu\text{eV}$  for better overall agreement. a,b) Adapted with permission.<sup>[14]</sup> Copyright 2017, American Physical Society.

showed that the three lowest-in-energy states in the  $D$  quintet are basically quasidegenerate with a splitting of about  $20 \mu\text{eV}$ , which is below the spectral linewidth. These three lines are of  $(\Gamma_3^+, \Gamma_4^+)$ ,  $\Gamma_5^+$  and  $(\Gamma_1^+, \Gamma_4^+)$  symmetry. The two other lines have  $(\Gamma_3^+, \Gamma_4^+)$  and  $\Gamma_5^+$  symmetry, and are split into two well-separated lines. For a comparison with experimental data, we expanded the model given in the study by Schweiner et al.<sup>[18]</sup> using a larger basis to obtain a higher accuracy for the resonance energies. This allows us not only to extend the calculations given in the study by Schweiner et al.<sup>[18]</sup> up to  $n = 6$ , but also to give  $D$  exciton energies up to  $n = 9$ , which are corroborated by a comparison with experimental data as discussed further below. By the extension up to  $n = 9$ , we enter the regime of Rydberg excitons which was not done so far in the study by Schweiner et al.<sup>[18]</sup> The calculated resonance energies of  $D$  excitons of the  $n = 3$  multiplet are indicated in Figure 1a by the cyan lines. The values are shown in Table 1. They are calculated using the Haken potential (see below) and are shifted here by a global offset of  $-237 \mu\text{eV}$  for better overall agreement. However, despite this offset, the relative splitting of the calculated  $D$  states agrees very well with the three lines observed in experiment.

According to symmetry considerations, all of the five  $D$  states can be accessed in OPA by electric field application. However, the

discrimination of the lowest three is not possible due to their small energy separation. Note that this direct comparison allows us to correct the assignment of  $D$  states given in the study by Schweiner et al.<sup>[18]</sup>

## 2.2. Details of the Hamiltonian

Although we find pairs of same symmetry among the five  $D$ , namely two states of  $\Gamma_5^+$ , two of  $(\Gamma_3^+, \Gamma_4^+)$  symmetry, these show very different binding energies. Hence, they are affected differently by the individual terms of the Hamiltonian. The influence of each term of the Hamiltonian to this level ordering and the corresponding state labeling was not discussed in detail so far and is deduced here based on the Hamiltonian given in the studies by Schweiner and co-workers<sup>[18,19]</sup> The resulting exciton-level scheme is shown in Figure 2 for the  $n = 3$  and  $n = 4$  multiplets, showing the evolution of the exciton fine structure from the Hamiltonian in spherical symmetry to the full cubic Hamiltonian and further including the exchange interaction from left to right. In addition, the exchange splitting of the green  $1S$  exciton is shown in the lower panel. The scheme is drawn according to numerical values calculated with the Hamiltonian shown in Table 1 and the comparison with the experiment from

**Table 1.** Numerically calculated exciton state energies divided into three contributions of the Hamiltonian (1). As dielectric correction  $H_\epsilon$ , the Haken potential is used. The states are labeled by their quantum numbers  $nL$ , their symmetry  $\Gamma_i^\pm$  and the main contribution of angular momentum  $F$ . Moreover, the green admixture of every state and the division into different admixtures of total angular momentum  $F$  are given. For some states, the sum of all admixtures might deviate from 100%. These deviations are below 1% and are mainly rounding errors. In addition, they might stem from higher  $F$ , e.g.,  $F = 9/2$ , which are not considered here. Note that  $F$  is the half integer quantum number of  $F = L + J$  except in the first column, where  $S, P, D, F$  denote the orbital angular quantum numbers  $L = 0 - 3$ .

$nL$	State		Energy [eV]			Green Adm. [%]	F [%]			
	$\Gamma_i^\pm$	$F$	$H_{\text{Hyd}} + H_d^s + H_\epsilon$	$+H_d^c$	$+H_{\text{exch}}$		1/2	3/2	5/2	7/2
1S <sup>e</sup>	$\Gamma_3^+, \Gamma_4^+$	3/2	2.187237	2.118795	2.118795					
1S <sup>e</sup>	$\Gamma_5^+$	3/2	2.187237	2.118795	2.154169					
3S	$\Gamma_2^+$	1/2	2.161730	2.159587	2.159587	0.5	99.5	0.0	0.0	0.5
3S	$\Gamma_5^+$	1/2	2.161730	2.159587	2.160714	4.2	71.7	5.1	22.5	0.6
3D	$\Gamma_3^+, \Gamma_4^+$	3/2	2.162462	2.162121	2.162121	0.3	0.0	96.6	3.1	0.1
3D	$\Gamma_5^+$	3/2	2.162462	2.162121	2.162150	0.3	0.2	96.1	3.5	0.0
3D	$\Gamma_1^+, \Gamma_4^+$	5/2	2.162485	2.162170	2.162170	0.3	0.0	0.0	99.8	0.1
3D	$\Gamma_3^+, \Gamma_4^+$	5/2	2.162485	2.162332	2.162332	0.4	0.0	3.4	96.5	0.0
3D	$\Gamma_5^+$	5/2	2.162485	2.162332	2.163286	7.0	19.1	8.4	72.0	0.4
3P	$\Gamma_8^-$	3/2	2.162361	2.161156	2.161156	1.0	0.0	98.9	0.7	0.1
3P	$\Gamma_7^-$	1/2	2.162353	2.161388	2.161388	0.7	99.3	0.0	0.0	0.1
4S	$\Gamma_2^+$	1/2	2.166379	2.165461	2.165461	0.2	99.8	0.0	0.0	0.2
4S	$\Gamma_5^+$	1/2	2.166379	2.165461	2.165834	1.4	80.1	2.5	17.0	0.3
4D	$\Gamma_3^+, \Gamma_4^+$	3/2	2.166668	2.166460	2.166460	0.2	0.0	96.0	3.8	0.0
4D	$\Gamma_5^+$	3/2	2.166668	2.166460	2.166478	0.2	0.3	96.7	2.8	0.0
4D	$\Gamma_1^+, \Gamma_4^+$	5/2	2.166684	2.168491	2.166490	0.2	0.0	0.0	99.9	0.1
4D	$\Gamma_3^+, \Gamma_4^+$	5/2	2.166684	2.166584	2.166584	0.2	0.0	4.0	96.0	0.0
4D	$\Gamma_5^+$	5/2	2.166684	2.166584	2.166991	3.0	17.4	4.3	78.0	0.2
4P	$\Gamma_8^-$	3/2	2.166633	2.166046	2.166046	0.5	0.0	99.4	0.4	0.1
4P	$\Gamma_7^-$	1/2	2.166630	2.166154	2.166154	0.3	99.5	0.0	0.0	0.2
4F	$\Gamma_7^-$	7/2	2.166696	2.166560	2.166560	0.1	0.2	0.0	0.0	99.8
4F	$\Gamma_8^-$	7/2	2.166696	2.166570	2.166570	0.1	0.0	0.1	45.9	54.0
4F	$\Gamma_8^-$	5/2	2.166696	2.166594	2.166594	0.1	0.0	0.0	54.0	45.9
4F	$\Gamma_6^-$	7/2	2.166696	2.166598	2.166598	0.1	0.0	0.0	48.1	51.9
4F	$\Gamma_6^-$	5/2	2.166696	2.166628	2.166628	0.1	0.0	0.0	51.9	48.1

Figure 1. Note that, the scale of splittings between lines does not correspond to the actual energy splittings, but is chosen schematically for best visualization.

The Hamiltonian as presented in the studies by Schweiner et al.<sup>[18,19]</sup> is given by

$$H = E_g + \frac{\gamma'_1 \mathbf{p}^2}{2m_0} - \frac{e^2}{4\pi\epsilon_0\epsilon r} + H_{\text{SO}} + H_d + H_{\text{CCC}} \quad (1)$$

with the relative momentum  $\mathbf{p}$  of electron and hole. The parameter  $\gamma'_1$  determines the reduced mass of the system  $m_0/\gamma'_1$ , where  $m_0$  is the electron mass in vacuum. The bandgap energy  $E_g$  is needed to lift the electron from the  $\Gamma_7^+$  valence band to the  $\Gamma_6^+$  conduction band. The parabolic kinetic energy term together with the screened Coulomb interaction with dielectric constant  $\epsilon$  and the spin-orbit interaction term  $H_{\text{SO}}$  form the hydrogen-like part of the Hamiltonian

$$H_{\text{Hyd}} = E_g + \frac{\gamma'_1 \mathbf{p}^2}{2m_0} - \frac{e^2}{4\pi\epsilon_0\epsilon r} + H_{\text{SO}} \quad (2)$$

The resulting spectrum consists of two independent hydrogen-like exciton series, i.e., the yellow and green series, which are characterized by the effective hole spin  $J = 1/2$  and  $J = 3/2$ , respectively.

This simple picture is modified by the influence of the  $H_d$  terms originating from the nonparabolicity of the valence bands and the central-cell corrections  $H_{\text{CCC}}$ , which describe corrections for small electron-hole separations. The  $H_d$  terms can be separated into a spherical and a cubic part,  $H_d = H_d^s + H_d^c$ . Similarly, the central-cell corrections consist of two parts, namely corrections to the dielectric constant for small excitons, that is primarily the Haken or Pollman-Büttner potential, and the exchange

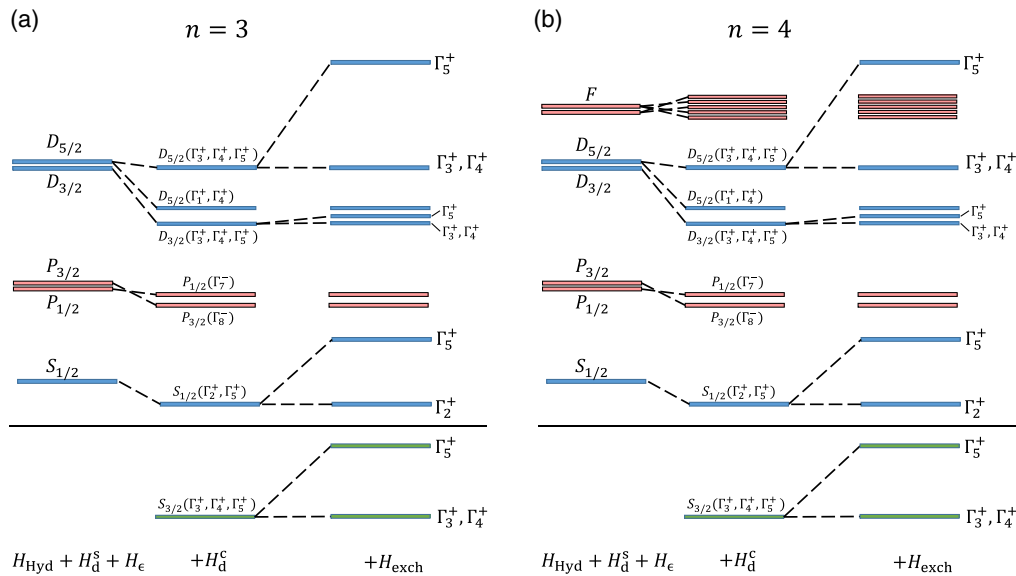


**Figure 2.** Schemes of the evolution of exciton fine structures of the a)  $n = 3$  and b)  $n = 4$  multiplets for the individual terms of the Hamiltonian (1), drawn according to numerical values shown in Table 1 and a comparison with experiment, as shown in Figure 1. The scale of splittings between the lines does not correspond to the actual energy splittings, but is chosen schematically for best visualization. Red colors denote odd parity  $P$  and  $F$  states, blue colors denote even parity  $S$  and  $D$  states of the yellow excitons. In addition, the green  $1S$  states are shown by green bars in the lowest panel of the middle and right columns each, where the influence of the coupling between yellow and green states on the multiplet splitting becomes important. The left columns in both panels show the levels when the details of the band structure are accounted for, but in a spherical approximation so that the sum of angular momenta  $F$  is a good quantum number. Levels with the same  $L$  are almost degenerate and can be described by a single quantum defect  $\delta_L$  (see text). The middle columns describe the level splitting when the cubic  $H_d^C$  term is added, which strongly mixes the yellow and green series. The states within a multiplet are shifted to lower energies and split into subgroups, now labeled by irreducible representations  $\Gamma_i^\pm$ . The right columns show the level splitting when the exchange interaction is included which splits the  $S$  and  $D$  excitons into *ortho* and *para* excitons. Correspondingly, yellow  $S$  states split into *ortho* ( $\Gamma_5^+$ ) and *para* ( $\Gamma_2^+$ ) excitons. The  $D$  excitons are affected by exchange as well due to their  $S$  admixture. A large *ortho*–*para* splitting between  $\Gamma_5^+$  and ( $\Gamma_3^+, \Gamma_4^+$ ) can be observed for excitons stemming from the  $D_{5/2}$  state, whereas the splitting is small for  $D_{3/2}$  states. For the  $n = 3$  multiplet, which comprises  $S$ ,  $P$ , and  $D$  excitons, the states belonging to the different shells ( $n, L$ ) remain in well-defined order. However, for the  $n = 4$  multiplet, the exchange splitting of the  $D_{5/2}$  is so large that the  $F$  exciton multiplet is fully embedded in between it and the  $D_{5/2}$  ( $\Gamma_5^+$ ) *ortho* exciton becomes the highest state of the multiplet.  $F$  states are not labeled for clarity.

interaction, which leads to a characteristic splitting between *ortho* and *para* states,  $H_{CCC} = H_e + H_{exch}$ .

The spherically symmetric description of the excitons is obtained by supplementing Equation (2) with the spherical band structure term and the modifications to the dielectric constant

$$H = H_{Hyd} + H_d^S + H_e \quad (3)$$

For this Hamiltonian, the sum of angular momenta  $\mathbf{F} = \mathbf{L} + \mathbf{J}$  remains a good quantum number. Accordingly, the states are labeled by  $L_F$  in this approximation. Note that the quantum number  $F$  for this angular momentum is not to be confused with the notation for states with  $L = 3$  envelope, which we call  $F$  states. Which of these is meant follows from the context.

The nonparabolicity of the band structure leads to a splitting of states with different  $L$ , whereby states with different  $M_L$  and  $M_J$  belonging to the same  $L$  are almost degenerate, as shown in the left column of Figure 2a. Using a quantum defect model, the binding energies can then be described by  $-\text{Ryd}/(n - \delta_L)^2$ , where  $\delta_L$  is the  $L$ -dependent quantum defect that decreases with increasing  $L$ , see the study by Schöne et al.<sup>[20]</sup> for details.

Next, we consider the cubic  $H_d^C$  term, that reduces the spherical symmetry of the Hamiltonian to the cubic symmetry  $O_h$  and

only the irreducible representations  $\Gamma_i^\pm$  remain as exact labels of the states, leading to a further splitting. The resulting level structure is shown in the middle column of Figure 2a. Due to the cubic contribution, the order of  $P$  states is flipped according to their total angular momenta  $F$ . The optically inactive  $P_{1/2}$  state is shifted above the optically active  $P_{3/2}$ . In contrast, the order of even parity states by increasing  $F$  from lower to higher energies is conserved. Note, the description given in Uihlein et al.<sup>[8]</sup> resulted in a reversed order of  $D_{5/2}$  and  $D_{3/2}$  excitons with the  $D_{3/2}$  being the highest state. In their model, the parameter controlling the strength of the spherical valence band term has the value  $\mu = 0.47$ , whereas the cubic terms are neglected,  $\delta = 0$ . As discussed in the study by Schweiner et al.,<sup>[19]</sup> a fit of the material parameters to band structure calculations<sup>[20,21]</sup> instead leads to the values  $\mu = 0.0586$  and  $\delta = -0.404$ . The discussion in this article is based on the latter values. We thus find that the contribution of the cubic terms to the splitting of states is much more pronounced than indicated in the study by Uihlein et al.,<sup>[8]</sup> whereas the spherical  $H_d^S$  term is less important. Accordingly, the assignment of the angular quantum number  $F$  has to be changed in the case of the  $D$  states, compared to the study by Uihlein et al.<sup>[8]</sup> We will discuss this in greater detail below.

Finally, the exchange interaction is added. It requires the additional consideration of the electron spin. Therefore, the magnetic quantum number of the electron  $M_{S_e}$  ceases to be a good quantum number. The total angular momentum of the exciton  $\mathbf{F}_t = \mathbf{F} + \mathbf{S}_e$  now characterizes the states. Affecting only excitons with an  $L = 0$  ( $S$ -like) component, the exchange leads to the well-known splitting into  $S$  *ortho* and  $para$  excitons,<sup>[22,23]</sup> corresponding to their electron- and hole-spin configurations. The *para* exciton of the yellow 1S has  $\Gamma_2^+$  symmetry and the *para* exciton of the green 1S has  $(\Gamma_3^+, \Gamma_4^+)$  symmetry. Both are pure spin-triplet states. Therefore, they are not affected by the exchange interaction. The *ortho* excitons have  $\Gamma_5^+$  symmetry and contain both spin-triplet and spin-singlet states. Due to exchange, they are shifted to higher energies, as shown in the right column of Figure 2a.

Since even parity states become mixed by the  $H_d$  terms of the Hamiltonian, also  $D$  states contain an  $L = 0$  part. As can be seen in the right column of Figure 2a, the two upper  $D$  states stemming from the  $D_{5/2}$  and the lower lying  $D_{3/2}$  states are split by the exchange interaction into an  $\Gamma_5^+$  and  $(\Gamma_3^+, \Gamma_4^+)$  component in the same way as the  $S$  excitons, in particular, the green 1S. Correspondingly, we refer to these states as  $D$ -envelope *ortho* and *para* excitons throughout this text. This denomination refers to the spin configuration of their  $L = 0$  admixture, which defines their response to exchange interaction. We justify this approach by the fundamental, to some extent dominant changes introduced by exchange.

Another example of spectra in electric field is shown in Figure 1b for the principal quantum number  $n = 4$ , where also the  $F$  excitons start to contribute. Without electric field, one observes the dipole-allowed  $P$  exciton and on its high-energy flank, the  $F$  exciton triplet, whereas on the low energy flank, the weak quadrupole-allowed signature of the  $S$  exciton is seen, as indicated in the left panel. In an electric field additional features appear, which carry the same signatures as described earlier for the  $D$  excitons: the low energy doublet, here between  $P$  and  $F$ , and another feature at higher energies, beyond the range of the  $F$  states. Similar to Figure 1a, we indicate the calculated energies and corresponding symmetries of the  $D$  excitons as given in Table 1 by cyan lines in the right panel for comparison, shifted by an overall offset of  $-218 \mu\text{eV}$  to lower energies. Again, the intrashell splitting agrees well with the observed lines in experiment: the three lower, almost degenerate, states match with the lowest one of the  $D$  lines observed in experiment, whereas the largely split  $D_{5/2}$  states match with the upper line of the doublet and the highest line, beyond the  $F$  states.

Remarkably, the fine structure splitting of the  $D_{5/2}$  excitons, in this case about  $400 \mu\text{eV}$ , is so large that the  $F$  exciton multiplet is enclosed in the split  $D$  multiplet. The splitting is even larger than the *ortho-para* splitting for the 4S states, which amounts to about  $370 \mu\text{eV}$ , see Table 1.

The level ordering of the  $n = 4$  multiplet is depicted in Figure 2b, again showing the evolution of the exciton fine structure from the spherical to the cubic Hamiltonian and further to the full model including exchange. As can be seen in the right column, the level ordering of angular momenta  $L$  as known from spherical symmetry, namely  $S$ ,  $P$ ,  $D$ , and  $F$ , is lifted for the  $n = 4$  multiplet: The highest state of this multiplet is the  $D_{5/2}(\Gamma_5^+)$  *ortho* exciton.

### 2.3. Coupling to the Green Series

The observation of the large fine structure splitting of the  $D$  excitons is the most important finding to be discussed in this article, as it is much larger than that of the  $P$  or  $F$  excitons. Therefore, it cannot be simply explained by the angular momentum dependence of the interaction matrix elements for the quadratic mixing of hole momenta (see aforementioned text), which would result in a monotonic scaling as  $(L + 1)^{-1}$ .

More advanced insight can be obtained from the analysis of the green content in yellow  $D$  excitons, as shown in Table 1. These values are calculated using the eigenvectors obtained from the diagonalization of the Hamiltonian (1), i.e., by calculating the expectation value of the projector into the  $J = 3/2$  space. It can be seen, that the amount of admixture of green 1S varies strongly among the different states within a multiplet and that the highest  $D$  exciton contains by far the highest content. In the following, we deduce the origin of the varying amounts of green admixture and its impact to the individual states.

The yellow-green mixing is highly relevant, because the 1S (*ortho*) exciton of the green series is located between the  $n = 2$  and  $n = 3$  excitons of the yellow series. As such, it is also important for the higher lying yellow excitons, located within a 10 meV range above the  $n = 3$  state. In contrast, the higher green excitons are not relevant for the mixing, as they are located at much higher energies, in the yellow exciton continuum.<sup>[24]</sup>

For becoming mixed, states need to have the same symmetry. As discussed earlier, the green 1S *ortho* exciton has symmetry  $\Gamma_5^+$  (see also the schemes in Figure 2). Indeed, the yellow 2S and 3S *ortho* excitons have the same symmetry, as do generally all  $nS$  excitons. Due to the interaction with the green 1S, the 2S is pushed to lower energies, whereas the 3S one is moved to higher energies.<sup>[23]</sup>

Among the 3D states, we find also two states with  $\Gamma_5^+$  symmetry, one stemming from  $D_{3/2}$  and one from  $D_{5/2}$  (see Figure 2), which can therefore undergo mixing with the green 1S *ortho* exciton, even without external electric field applied. However, they show very different degrees of mixing. The first one has only 0.3% green content, whereas the latter one has a green content of 7.0%, see Table 1.

This difference in green content can be understood now by analyzing the total angular momentum  $F$  of the involved states. As mentioned above, an earlier analysis was given in the study by Uihlein et al.,<sup>[8]</sup> where the strong mixing of the energetically highest  $D$  exciton with the green 1S exciton compared to all other states within a multiplet was related to the spherical band structure terms. For excitons of the green series, one finds  $J = 3/2$ , and in particular,  $F = 3/2$  for the green  $1S_{3/2}$  exciton. As the spherical terms preserve  $F$ , the  $D_{3/2}$  excitons are the only candidates that are mixed with the green  $1S_{3/2}$  exciton already by the spherical part of the Hamiltonian (Equation (3)) explaining their large amount of green content in the description given in the study by Uihlein et al.<sup>[8]</sup> Accordingly, the  $D_{5/2}$  excitons have a lower content of green  $1S_{3/2}$  in that model and the level repulsion between the green  $1S_{3/2}$  state and the  $D_{3/2}$  states then lifts the latter above the  $D_{5/2}$  states.

However, as indicated in the aforementioned discussion of the Hamiltonian, the actual material parameters of  $\text{Cu}_2\text{O}$  lead to a much weaker spherical  $H_4^s$  term<sup>[19]</sup> and a much more important cubic  $H_4^c$  term, compared to the assumptions by Uihlein et al.<sup>[8]</sup> We can understand how this changes the picture as explained in the following. Let  $\Pi'$  denote the quantum numbers of the green  $1S_{3/2}$  state, such as  $L' = 0$ ,  $J' = 3/2$ , and  $F' = 3/2$ , and  $\Pi$  denote the quantum numbers of a state from the yellow series such as  $L$ ,  $J = 1/2$ , and  $F$ . The matrix elements belonging to the dominant cubic  $H_4$  term were presented in the study by Schweiner et al.<sup>[19]</sup> The derived expression depends upon a certain Wigner  $9j$  symbol as follows

$$\langle \Pi' | [P^{(2)} \times I^{(2)}]_q^{(4)} | \Pi \rangle = A_{\Pi', \Pi, q} \begin{Bmatrix} L' & L & 2 \\ J' & J & 2 \\ F' & F & 4 \end{Bmatrix} \quad (4)$$

where  $A_{\Pi', \Pi, q}$  is an abbreviation for the part of the formula we are not interested in for our discussion. The parameter  $q$  controls the behavior under rotations, and is not important here. The angular momenta and spins appearing in the  $9j$  symbols must fulfill certain selection rules, otherwise the matrix element vanishes. One of the conditions is that the angular momenta in each row satisfy the triangular inequalities of angular momentum coupling. From the second row, we can thus deduce that the matrix element vanishes for  $J' = J = 1/2$ . The effect of the cubic terms on the yellow series thus crucially depends upon the coupling to the green series. The green  $1S$  state has  $L' = 0$  and  $F' = 3/2$ . From the first and third rows, we can then conclude that it can only directly be coupled to states with  $L = 2$  and  $F \geq 5/2$ , i.e., to the  $D_{5/2}$  excitons. For any other yellow state, and in particular, for the  $D_{3/2}$  states, the matrix element vanishes. As a consequence, the level repulsion from the green  $1S$  caused by the cubic terms most strongly affects the  $D_{5/2}$  lines, lifting them above the  $D_{3/2}$  lines. This is also consistent with the ( $D_{5/2}(\Gamma_1^+, \Gamma_4^+)$ ) exciton staying energetically very close to the  $D_{3/2}$  lines, as it cannot be repelled by the green states of different irreducible representation. This understanding of the energetic order of the states with different  $F$  values is corroborated by the numerically calculated  $F$  admixtures shown in Table 1, which are calculated analogously to the green admixtures.

Moreover, due to the mixing between yellow  $D$  states and the green  $1S$  exciton by the Hamiltonian, the former also gain  $L = 0$  character and become, therefore, sensitive to exchange interaction that splits  $S$ -like states into *ortho* and *para* excitons. Its effect on  $D$  states is important, in particular, as the green exchange energy is large, causing, for example, a more than 30 meV splitting between the green  $1S$  *ortho* and *para* excitons in comparison with only 12 meV for the corresponding yellow states. Hence, in addition to level repulsion from the green  $1S$ , the difference of green admixture finally results in a different exchange splitting of the  $D_{3/2}$  and  $D_{5/2}$  states. While the first one is only barely affected by exchange due to its small green fraction, the latter shows a pronounced exchange splitting caused by its larger green admixture, as discussed earlier.

These considerations are substantiated by the analysis for  $n = 4$ , where the  $D_{5/2}(\Gamma_5^+)$  *ortho* exciton has again the largest

green content of 3.0% compared to about 0.2% for all other  $D$ -envelope states, see Table 1. Consequently, this state is shifted even above the  $F$  exciton multiplet.

## 2.4. Extrapolation to $n \geq 6$

As discussed earlier, the strong shift of the  $D_{5/2}(\Gamma_5^+)$  *ortho* exciton to higher energies renders it the highest state of a multiplet, as it was shown for  $n = 3$  and 4 before. Here, we confirm this for the multiplet of  $n = 6$ , where in addition,  $H$  excitons can be observed, the highest angular momentum states observed so far: In **Figure 3**, the position of  $6H$  states is indicated, which is well known from high-resolution laser spectroscopy.<sup>[12]</sup> Indeed, the  $D_{3/2}(\Gamma_5^+)$  appears at an even higher energy, as indicated by the dashed blue arrow in the left panel of **Figure 3**.

This observation is corroborated by extending the calculations made in the study by Schweiner et al.<sup>[18]</sup> up to the  $n = 6$  multiplet. The obtained fine structure of  $n = 6$  states is shown in **Figure 4**. The states are spread over an energy range of about 400  $\mu\text{eV}$  beginning from the  $S_{1/2}(\Gamma_2^+)$  *para* exciton at the lowest energy up to the  $D_{5/2}(\Gamma_5^+)$  *ortho* exciton at highest energy. The color coding from white to green indicates the admixture of green  $1S_{3/2}$  state to each state in the multiplet. As shown, the yellow  $S_{1/2}$  and  $D_{5/2}$  *ortho* states contain the largest green fraction. Although the green content is below 1%, it still induces a splitting onto the  $D_{5/2}$  exciton, shifting its *ortho* component to higher energies and even above the  $G$  and  $H$  states of this multiplet. The large green content of the yellow  $S_{1/2}$  *ortho* state is explained by the mixing between the green and yellow  $S$  *ortho* excitons caused by the exchange interaction.

Now, we compare the observed  $D$  exciton splittings in experiment to the calculated values using the full Hamiltonian (1) as a

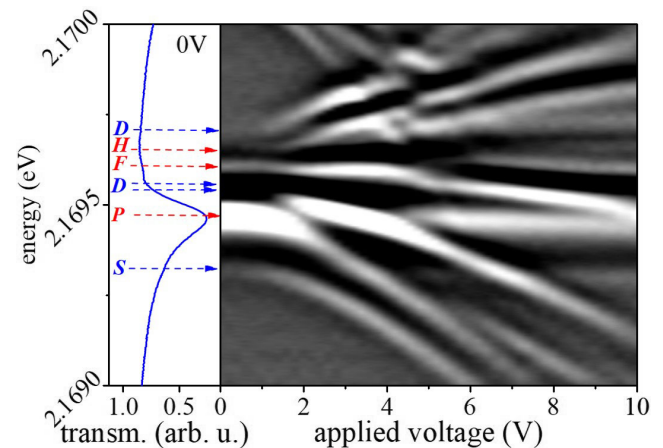


**Figure 3.** Contour plot of the second derivative of transmission spectra of  $n = 6$  multiplet as a function of applied bias. The left panel shows a reference spectrum for zero bias and labels of different exciton states. Blue lines indicate even excitons, red lines odd excitons. For  $n = 6$  also  $H$  excitons with  $L = 5$  contribute to the multiplet, as indicated in the left panel. Under the application of an electric field, another line appears on the high energy side of the  $H$  exciton, that can be identified as the  $D_{5/2}(\Gamma_5^+)$  *ortho* exciton. Adapted with permission.<sup>[14]</sup> Copyright 2017, American Physical Society.

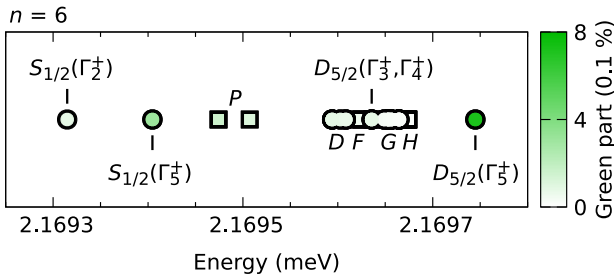


**Figure 4.** Calculated exciton energies for the multiplet of principle quantum number  $n = 6$  using the Haken potential. The color coding indicates the content of the green  $1S$  exciton. The  $S$  and  $D$  ortho excitons of  $\Gamma_5^+$  symmetry show the largest admixture and are moved to higher energies. As a result, the  $D_{5/2}(\Gamma_5^+)$  exciton is shifted to an energy higher than the  $H$  excitons which renders it the highest state of the multiplet.

function of principal quantum number  $n$ . The amount of green admixture depends on the form of the dielectric correction  $H_e$ , as it was shown in the study by Schweiner et al.,<sup>[18]</sup> namely the Haken– or the Pollman–Büttner potential. Both models lead to slightly different values for the resonance energies of exciton states and  $D_{5/2}$  intrashell splitting, as the amount of green admixture differs in each case. Compared with the Haken potential, the green admixture to yellow states is about a factor of two less using the Pollmann–Büttner potential, as can be seen in the study by Schweiner et al.<sup>[18]</sup> However, also for the Pollmann–Büttner potential, these admixtures are still much larger than for any other angular momentum state in the exciton multiplet belonging to a particular  $n$  and the  $D_{5/2}$  becomes the highest state of a multiplet for the Pollmann–Büttner potential as well.

The measured  $D_{5/2}$  ortho–para splittings are shown by red crosses in Figure 5a as a function of the principal quantum number. Unfortunately, the range of accessible  $n$  is limited in our studies, as the experimental resolution is not good enough to determine the splittings beyond  $n = 5$ . For higher  $n$ , the lower two  $D$  lines cannot be clearly identified within the Stark–fan in an electric field due to their spectral proximity to the prominent  $P$  and  $F$  states and their small oscillator strength (see Figure 3, showing  $n = 6$ ).

The splitting of the  $D_{5/2}$  states is found to agree even quantitatively with the predictions by the Haken potential (squares), whereas the Pollmann–Büttner potential (circles) slightly underestimates the splitting.

In contrast to the low-energy  $D$  lines, the strongly shifted  $D_{5/2}(\Gamma_5^+)$  ortho exciton can be identified in experimental spectra up to  $n = 9$ . The obtained splitting between this state and the dipole-allowed  $P_{3/2}$  exciton of each multiplet is shown in Figure 5b, again in comparison with the predictions by the full Hamiltonian using Haken (squares) and Pollmann–Büttner potentials (circles). In this case, the Pollmann–Büttner potential gives a better agreement than the Haken potential. The latter one slightly overestimates the shown splitting.

Despite the differences on a quantitative level, both approximations show a consistent trend of a strong decrease in the strength of the splitting energy with increasing principal quantum number. As discussed earlier, two factors are relevant for the energy splitting: the complex valence band dispersion that mixes

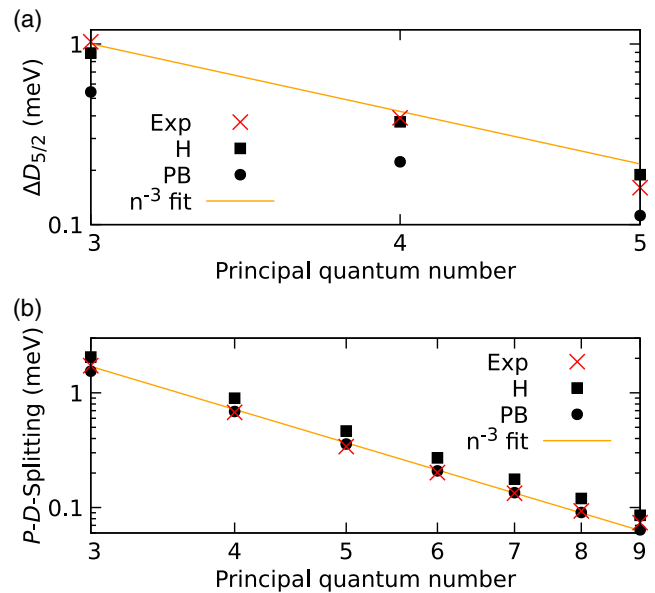


**Figure 5.** a) Exchange splitting between the  $D_{5/2}$  ortho and para excitons versus principal quantum number. For definition of  $D$  ortho and para excitons, see text. b) Splitting between  $D_{5/2}(\Gamma_5^+)$  ortho exciton, the highest one in the multiplet, and the dipole-allowed  $P_{3/2}$  exciton versus principal quantum number. In both panels, the red crosses show the experimental data. Black symbols give calculated results using the Haken (squares) and Pollmann–Büttner (circles) potentials. The yellow lines give a fit to the experimental data, following  $n^{-3}$ .

the yellow and green series, in total, described by the terms  $H_{\text{Hyd}} + H_d^s + H_d^c + H_e$ , as well as the exchange interaction  $H_{\text{exch}}$ . The matrix elements describing the first part can be shown to scale as  $n^{-3}$ <sup>[13]</sup> and also the exchange interaction shows a characteristic scaling with  $n$ : In a simplified model using hydrogen wavefunctions, it is expected to scale as  $n^{-3}$  as well.<sup>[22]</sup> Indeed, the data can be well described by a corresponding fit with  $n^{-3}$ , shown by the yellow line in Figure 5a.

As all interaction mechanisms included in the full Hamiltonian (1) that are defining the fine structure of a multiplet scale in a good approximation as  $n^{-3}$  (see earlier text), the level ordering found for  $n = 3 - 6$  can be extrapolated to higher  $n$  and the  $D_{5/2}(\Gamma_5^+)$  ortho exciton is expected to be the highest state of all multiplets even in the high- $n$  regime.

### 3. Conclusion

We have discussed the origin of the large fine structure splittings of the yellow  $D$  exciton multiplets in cuprous oxide and assigned it to the strong mixing of the  $D_{5/2}$  state of  $\Gamma_5^+$  symmetry with the green  $1S_{3/2}$  exciton of the same symmetry, in agreement with theoretical calculations. Extended calculations up to the multiplet of  $n = 9$  showed that this state is the energetically highest state of each exciton multiplet. Hence, the ordering of states by increasing angular momentum  $L$  is lifted in  $\text{Cu}_2\text{O}$ .

Recent studies discussed the sensitivity of highly excited Rydberg excitons with quantum numbers  $n > 10$  to electric fields induced by charged impurities.<sup>[5,16]</sup> As even parity  $D$  states are



optically activated by electric fields, the results of this article play an important role for future investigations concerning exciton–impurity interactions. Due to its scaling according to  $n^{-3}$ , the even-exciton multiplet structure obtained here at low  $n$  can be extrapolated to the high- $n$  regime and can be helpful for the analysis and interpretation of impurity-dominated spectra, in particular close to the bandgap.

Furthermore, the detailed insight into the  $D$  exciton fine structure, corroborated by the deduction of the total angular momenta  $F$  contributing to the  $D$  exciton wavefunctions, is highly relevant for the investigation of plasmon scattering rates between excitons of different angular momenta<sup>[25]</sup> or possible microwave-driven intraband transitions.<sup>[26]</sup>

## Acknowledgements

The authors acknowledge the financial support by the Deutsche Forschungsgemeinschaft through the International Collaborative Research Centre TRR160 (project number: 249492093, project: A8) and through grant no. MA 1639/13-1.

Open access funding enabled and organized by Projekt DEAL.

## Conflict of Interest

The authors declare no conflict of interest.

## Data Availability Statement

The data that support the findings of this study are available on request from the corresponding author.

## Keywords

high-resolution spectroscopy, Rydberg excitons, semiconductors

Received: June 21, 2021

Revised: September 2, 2021

Published online: October 4, 2021

- [1] a) C. Klingshirn, *Semiconductor Optics*, Springer, Berlin/Heidelberg, Germany **2012**; b) M. Grundmann, *The Physics of Semiconductors*, Springer **2016**.
- [2] G. Wang, A. Chernikov, M. M. Glazov, T. F. Heinz, X. Marie, T. Amand, B. Urbaszek, *Rev. Mod. Phys.* **2018**, *90*, 021001.
- [3] M. A. Becker, R. Vaxenburg, G. Nedelcu, P. C. Sercel, A. Shabaev, M. J. Mehl, J. G. Michopoulos, S. G. Lambrakos, N. Bernstein, J. L. Lyons, T. Stöferle, R. F. Mahrt, M. V. Kovalenko, D. J. Norris, G. Rainò, A. L. Efros, *Nature* **2018**, *553*, 189.
- [4] A. V. Rodina, A. A. Golovatenko, E. V. Shornikova, D. R. Yakovlev, *Phys. Solid State* **2018**, *60*, 1537.
- [5] S. O. Krüger, H. Stolz, S. Scheel, *Phys. Rev. B* **2020**, *101*, 235204.
- [6] H. Stolz, F. Schöne, D. Semkat, *New J. Phys.* **2018**, *20*, 023019.
- [7] D. Fröhlich, R. Kenklies, Ch. Uihlein, C. Schwab, *Phys. Rev. Lett.* **1979**, *43*, 1260.
- [8] Ch. Uihlein, D. Fröhlich, R. Kenklies, *Phys. Rev. B* **1981**, *23*, 2731.
- [9] S. Zielińska-Raczyńska, G. Czajkowski, D. Ziemkiewicz, *Phys. Rev. B* **2016**, *93*, 075206.
- [10] T. Kazimierczuk, D. Fröhlich, S. Scheel, H. Stolz, M. Bayer, *Nature* **2014**, *514*, 343.
- [11] M. A. M. Versteegh, S. Steinhauer, J. Bajo, T. Lettner, A. Soro, A. Romanova, S. Gyger, L. Schweickert, A. Mysyrowicz, V. Zwiller, arXiv:2105.07942, **2021**.
- [12] J. Thewes, J. Heckötter, T. Kazimierczuk, M. Aßmann, D. Fröhlich, M. Bayer, M. A. Semina, M. M. Glazov, *Phys. Rev. Lett.* **2015**, *115*, 027402.
- [13] J. Heckötter, M. Freitag, D. Fröhlich, M. Aßmann, M. Bayer, M. A. Semina, M. M. Glazov, *Phys. Rev. B* **2017**, *96*, 125142.
- [14] J. Heckötter, M. Freitag, D. Fröhlich, M. Aßmann, M. Bayer, M. A. Semina, M. M. Glazov, *Phys. Rev. B* **2017**, *95*, 035210.
- [15] F. Schweiner, J. Main, G. Wunner, M. Freitag, J. Heckötter, Ch. Uihlein, M. Aßmann, D. Fröhlich, M. Bayer, *Phys. Rev. B* **2017**, *95*, 031202.
- [16] J. Heckötter, D. Janas, R. Schwartz, M. Aßmann, M. Bayer, *Phys. Rev. B* **2020**, *101*, 235207.
- [17] S. Lynch, C. Hodges, S. Mandal, W. Langbein, R. Singh, L. Gallagher, J. Pritchett, D. Pizzey, J. Rogers, C. Adams, M. Jones, *Phys. Rev. Mater.* **2021**, *5*, 084602.
- [18] F. Schweiner, J. Main, G. Wunner, C. Uihlein, *Phys. Rev. B* **2017**, *95*, 195201.
- [19] F. Schweiner, J. Main, M. Feldmaier, G. Wunner, Ch. Uihlein, *Phys. Rev. B* **2016**, *93*, 195203.
- [20] F. Schöne, S.-O. Krüger, P. Grünwald, H. Stolz, S. Scheel, M. Aßmann, J. Heckötter, J. Thewes, D. Fröhlich, M. Bayer, *Phys. Rev. B* **2016**, *93*, 075203.
- [21] M. French, R. Schwartz, H. Stolz, R. Redmer, *J. Phys.: Condens. Matter* **2009**, *21*, 015502.
- [22] P. Rommel, J. Main, A. Farenbruch, D. Fröhlich, D. R. Yakovlev, M. Bayer, *Phys. Rev. B* **2021**, *103*, 075202.
- [23] A. Farenbruch, D. Fröhlich, D. R. Yakovlev, M. Bayer, *Phys. Rev. Lett.* **2020**, *125*, 207402.
- [24] P. Rommel, P. Zielinski, J. Main, *Phys. Rev. B* **2020**, *101*, 075208.
- [25] H. Stolz, D. Semkat, *J. Phys.: Condens. Matter* **2021**, *33*, 425701.
- [26] L. A. P. Gallagher, J. P. Rogers, J. D. Pritchett, R. A. Mistry, D. Pizzey, C. S. Adams, M. P. A. Jones, P. Grünwald, V. Walther, C. Hodges, W. Langbein, S. A. Lynch, arXiv: 2109.09614, **2021**.